Original Research

E2F3 drives the epithelial-to-mesenchymal transition, cell invasion, and metastasis in breast cancer

Shirley Jusino[1], Yainyrette Rivera-Rivera[1], Camille Chardón-Colón[2], Armando J Ruiz-Justiz[3] (iD), Jaleisha Vélez-Velázquez[3], Angel Isidro[4], Melanie E Cruz-Robles[5], Margarita Bonilla-Claudio[1], Guillermo N Armaiz-Pena[1] and Harold I Saavedra[1] (iD)

[1]Department of Basic Sciences, Division of Pharmacology and Cancer Biology, Ponce Health Sciences University-Ponce Research Institute, Ponce 00716-2348, Puerto Rico; [2]Department of Basic Sciences, Division of Biochemistry, Ponce Health Sciences University-Ponce Research Institute, Ponce 00716-2348, Puerto Rico; [3]Department of Biology, University of Puerto Rico-Ponce, Ponce 00716, Puerto Rico; [4]Department of Basic Sciences, Division of Physiology, Ponce Health Sciences University-Ponce Research Institute, Ponce 00716-2348, Puerto Rico; [5]Department of Basic Sciences, Division of Microbiology, Ponce Health Sciences University-Ponce Research Institute, Ponce 00716-2348, Puerto Rico
Corresponding author: Harold I Saavedra. Email: hsaavedra@psm.edu

Impact statement

The results described here will impact TNBC patients, since there are no targeted therapies against this deadly subtype of breast tumors. Our results suggest that kinases that are regulated by E2F3 or impinge on SGO1 phosphorylation are potential targets for future treatment of TNBC.

Abstract

E2F3 is a transcription factor that may initiate tumorigenesis if overexpressed. Previously, we demonstrated that E2F3 mRNA is overexpressed in breast cancer and that E2F3 over-expression results in centrosome amplification and unregulated mitosis, which can promote aneuploidy and chromosome instability to initiate and sustain tumors. Further, we demonstrated that E2F3 leads to overexpression of the mitotic regulator Shugoshin-1, which until recently had unknown roles in cancer. This study aims to evaluate the roles of E2F3 and Shugoshin-1 in breast cancer metastatic potential. Here we demonstrated that E2F3 and Shugoshin-1 silencing leads to reduced cell invasion and migration in two mesenchymal triple-negative breast cancer (TNBC) cell lines (MDA-MB-231 and Hs578t). Moreover, E2F3 and Shugoshin-1 modulate the expression of epithelial-to-mesenchymal transition-associated genes such as Snail, E-Cadherin, and multiple matrix metalloproteinases. Furthermore, E2F3 depletion leads to reductions in tumor growth and metastasis in NOD-*scid* Gamma mice. Results from this study suggest a key role for E2F3 and a novel role for Shugoshin-1 in metastatic progression. These results can further help in the improvement of TNBC targeted therapies by interfering with pathways that intersect with the E2F3 and Shugoshin-1 signaling pathways.

Keywords: E2F3, Shugoshin-1, triple-negative breast cancer, epithelial-to-mesenchymal transition, invasion

Introduction

Breast cancer is the most common cancer diagnosed in women worldwide.[1] Despite significant advancements and new treatment options, breast cancer remains the leading cause of cancer-related deaths in women.[1] Especially deadly are basal, triple-negative breast cancers (TNBC) to which there are no effective biological therapies available because they lack the estrogen, progesterone, and Her2 receptors. Our laboratory focuses on the study of the E2F pathway as a possible target against TNBC. E2F3 belongs to the E2F family of transcription factors, which are divided into three major groups: activators (E2F1, E2F2, and E2F3a), canonical repressors (E2F3b-E2F6), and atypical repressors (E2F7 and E2F8) of gene transcription.[2] E2F activators promote gene transcription and have been shown to act as oncogenes, while the canonical and the atypical repressors halt gene transcription and behave as tumor suppressors.[2] However, their activity and function can be tissue and context-dependent.

Our group and others have shown a role for E2Fs in tumorigenesis and tumor maintenance.[3] For example, we showed that E2F3 is overexpressed in breast cancer, and maintains higher rates of centrosome amplification and dysregulated mitosis, which promotes aneuploidy and chromosome instability to initiate and sustain tumors.[4–7] Recent studies have shown a novel role for E2Fs in tumor progression, including epithelial-to-mesenchymal transition (EMT) signaling, invasion, and metastasis.[2,8,9] EMT is a process characterized by the loss of epithelial junctions (adherence junctions, gap junction, tight junction, and desmosomes) and apical-basal polarity[10–12] that result in cytoskeleton reorganization and morphological changes. These morphological changes are caused by changes in protein expression like the loss of epithelial markers that maintain cell adhesion (E-Cadherin, ZO-1, among others), upregulation of mesenchymal markers that favor migration (N-Cadherin, Vimentin, among others), and matrix metalloproteinases (MMPs) that enhance extracellular matrix (ECM) degradation and enable cell invasion.[13–16] Most of these molecular changes are mainly orchestrated by EMT transcription factor families such as SNAIL,[17] bHLH (which include Twist1),[18] ZEB,[10,15] and many others. Ultimately, EMT results in the acquisition of mesenchymal features that allow cells to invade and migrate through the ECM. EMT is a process that occurs naturally in embryological development but is observed in pathological states such as cancer and fibrosis.[10] Although EMT signaling has been thoroughly studied, several knowledge gaps remain, such as identifying key EMT drivers in cancer and developing strategies to target these to stop the metastatic process.

Our group has shown that E2F3 overexpression leads to the upregulation of mitotic kinases such as TTK (also known as Mps1) and NEK2, as well as mitotic regulators such as Shugoshin-1 (SGO1).[6,19] Our laboratory and others have shown that some mitotic kinases such as TTK and Nek2 have a role in EMT and invasion in breast cancer and other cancers.[19–23] SGO1 is a common target of these kinases.[24] However, the exact mechanism of how E2F3 and SGO1 regulate EMT in TNBC remains poorly understood. Hence, we investigated the effects of E2F3 and SGO1 depletion in EMT, cell invasion, and cell migration in TNBC to dissect the underlying mechanism behind this observation. We hypothesized that E2F3 and SGO1 depletion will restore the expression of epithelial genes (e.g. E-Cadherin) and decrease the expression of mesenchymal genes (e.g. Vimentin, Snail, among others), therefore, decreasing cell invasion, migration, and metastasis. To test our hypothesis, we silenced E2F3 and SGO1 in TNBC cells and evaluated their effects on EMT signaling and functional processes such as cell–cell invasion and migration *in vitro*. Further, we evaluated the effects of E2F3 depletion in an orthotopic mouse model of breast cancer metastasis using Nod-*scid* Gamma (NSG) mice. Our results showed that E2F3 and SGO1 knockdown modulated EMT protein levels and protein localization, as well as decreased MMP2, MMP3, and MMP9 mRNA levels. These EMT-associated changes led to reduced cell invasion, migration, and metastasis. In summary, these results suggest a key role for E2F3 and a novel role for SGO1 in breast cancer progression. This is the first study that demonstrates a role for E2F3 and SGO1 as drivers of EMT and cell invasion in TNBC.

Materials and methods

Bioinformatic analyses

Expression of E2F3 and SGO1 was evaluated in TCGA PanCancer Atlas and METABRIC databases using cBioPortal (http://www.cbioportal.org/). Survival outcomes in breast cancer patients were investigated using z-scores with a threshold set at 2 in KM plotter (https://kmplot.com/analysis/).[25] We used the Jetset feature to choose the optimal genomic probes for E2F3 or SGO1. Survival outcomes for relapse-free survival (RFS), overall survival (OS), post-progression survival (PPS), and distant metastasis-free survival (DMFS) were evaluated. Furthermore, E2F3 or SGO1 expression on invasive ductal breast cancer was compared to normal breast tissue using Oncomine (https://www.oncomine.org/resource/login.html). Here, Curtis (METABRIC) and TCGA databases were used. Finally, an in silico analysis for protein–protein interaction networks was done to correlate E2F3, SGO1, and selected EMT genes. For this analysis, we used STRING (http://www.string-db.org). We are reporting evidence, confidence, and molecular action for these interactions. The interpretation of those networks is as follows: nodes: number of proteins in the network; edges: number of interactions within the proteins; node degree: average number of interactions within proteins; clustering coefficient: denotes the tendency of the network to form clusters (the closer this value is to 1, the more likely it is to form clusters); and protein–protein interaction enrichment *P*-value: denotes the statistical significance. Proteins are considered hubs when they overpass the average interactions (n° interactions > node degree).

Cell culture

MCF10A (CRL-10317), MDA-MB-231 (HTB-26), and Hs578t (HTB-126) cell lines were purchased from ATCC and cultured as described in Lee *et al.*[19] MCF10A cells overexpressing E2F3 (MCF10A E2F3) or control (MCF10A) were developed in our laboratory using a pBABE-*hygro* backbone and were cultured following specifications described in Lee *et al.*[19] MDA-MB-231 cells with shRNA E2F3 (Target sequence: CCAACTCAGGACATAGCGATT, Clone ID: TRCN0000013807, Sigma-Aldrich) or shRNA Control (SHC002V, Sigma-Aldrich) were developed using pLKO.1 transduction lentiviral particles and cultured in Dulbecco's Modified Eagle's Medium (DMEM) (30–2002, ATCC) with 10% fetal bovine serum (FBS) (30–2020, ATCC), 5% pen strep (11074440001, Sigma-Aldrich), and 6 μg of puromycin dihydrochloride (P9620-10ML, Sigma-Aldrich).

RNA interference

For MDA-MB-231 and Hs578t transient transfections, we seeded 150,000 cells/mL in a six-well plate and allowed them to attach overnight. After 24 h, when confluency

was approximately 60–80%, cells were transfected using 50 nM ON-TARGET plus Human siRNAs from Dharmacon for E2F3 (L-003261–00-0005), SGO1 (L-015475–00-0005), MMP3 (L-005968–00-0005), or Snail (L-010847–01-0010). A scrambled siRNA sequence (Silencer negative control siRNA, AM4611, Invitrogen) was used as control. The siRNA sequences were mixed with jetPRIME Transfection Reagent (114–07, Polyplus) in cell media according to manufacturer instructions. The cells were incubated with the transfection complex for 48 h and used for the experiments described below.

Western blotting

Cell protein lysates were prepared and Western blotting was performed according to our published protocols (Lee et al.[19]) The following primary antibodies were used: E2F3 (ab50917 from Abcam, sc-878 from Santa Cruz Biotechnology, and E8651 from Sigma-Aldrich), SGO1 (ab58023 from Abcam and sc-393993 from Santa Cruz Biotechnology), ZO-1 (8193 s, Cell Signaling), N-Cadherin (610920, BD Transduction Laboratories), E-Cadherin (3195 s, Cell Signaling), Vimentin (5741 s, Cell Signaling), Slug (9585 s, Cell Signaling), Snail (3879 s, Cell Signaling), and Twist1 (46702 s, Cell Signaling). β-actin (sc-47778, Santa Cruz Biotechnology) was used as a loading control. For secondary antibodies, either goat anti-rabbit HRP (sc-2004, Santa Cruz Biotechnology) or goat anti-mouse HRP (NXA931, GE Healthcare) was used. Signals were detected by using a Lumigen TMA-6 reagent (Lumigen Inc., Southfield, MI).

RNA isolation, RNA quantification, and quantitative real-time PCR

Forty-eight hours post-transfection, total RNA from each cell sample was extracted using the RNeasy Mini kit (1002137, Qiagen) following the manufacturer's instructions. The absorbance ratios at 260/280 nm of the isolated RNA samples were measured using a NanoDrop 2000c spectrophotometer (Thermo Fisher) and an aliquot of 1 μg total RNA was subjected to a reverse transcriptase reaction using the iScript cDNA Synthesis kit (1708891, BioRad) in an S1000 Thermocycler (BioRad). A qPCR analysis was performed using a Realplex Eppendorf machine. We used the following RT^2 qPCR primers from Qiagen: human E2F3 (PPH00917F-200), SGO1 (PPH10976A-200), SNAI1 (PPH02459B-200), MMP2 (PPH00151B-200), MMP3 (PPH00235F-200), MMP9 (PPH00152E-200), and GAPDH (PPH72843A-200). Each primer was mixed with cDNA and iQ SYBR Green Supermix (1708880, BioRad) and subjected to 40 cycles using a Realplex2 (ThermoFisher). The data reported here is the average of three independent experiments. The fold change for each gene relative to the control group was determined using the $2^{-\Delta\Delta CT}$ method.

In vitro invasion and migration assays

Invasion and migration of MCF10A, MDA-MB-231, or Hs578t cells were assayed using BioCoat Matrigel Invasion Chambers (354480, Corning) and BioCoat Control Cell Culture Inserts (354578, Corning) respectively,

following established protocols in our laboratory.[20] Images were taken at a magnification of 200× and 400×. A total of 12 fields/groups (4 fields/treatment on each experiment) were counted by light microscopy using the Nikon DS-Ri2 microscope. The mean of invading and migrating cells was calculated from three independent experiments.

Immunofluorescence and image acquisition

MDA-MB-231 and Hs578t cells were plated at a density of 40,000 cells/well in 8-well slides (08–774-26, Fisher Scientific), allowed to attach overnight, and processed as described.[19] The cells were stained with primary antibody (at a dilution of 1:100) against E-Cadherin (3195 s, Cell Signaling or 610181, BD Transduction Laboratories) and Vimentin (5741 s, Cell Signaling). Secondary antibody, either Alexa Fluor 555-conjugated goat anti-rabbit (A21428, Life Technologies) or Alexa Fluor 488-conjugated goat anti-mouse (A11029, Life Technologies), was diluted 1:1000 in PBS and incubated for 1 h at room temperature. DAPI (1 mg/mL) was applied as nuclear staining. Cells were washed once with 1× PBS for 5 min. All fixed samples were mounted in Fluorogel mounting medium. Images were taken at a magnification of 600× using the Nikon DS-Ri2 microscope.

Immunohistochemistry

Breast cancer tissue arrays (BC081120e) were purchased from US Biomax and stained for E2F3 (ab50917, Abcam) and SGO1 (sc-393993, Santa Cruz Biotechnology) as previously described in King et al.[20] Images were taken using the microscope Nikon DS-Ri2 at a magnification of 200× and 400×. Then, .tiff images were imported into the Definiens Tissue Studio v4.2 suite (Definiens Inc, Germany) for segmentation and analysis. In Tissue Studio, Cell and Marker Area segmentation algorithms were used to quantify the amount and intensity (negative, low, moderate, or high) of positive IHC staining. The data for each core were exported into Microsoft Excel and H-Score was determined using the data for low, moderate, and high-intensity staining. Cytoplasmic and nuclear staining was reported for hormone receptor-positive tissues ($n = 71$), hormone receptor-negative tissues ($n = 29$), or normal adjacent tissue ($n = 10$). These images were independently evaluated by a certified pathologist (Dr. Ángel Isidro, M.D.) at Ponce Health Sciences University.

Cell counting kit-8 assay

Two thousands cells of MDA-MB-231 shRNA Control and shRNA E2F3 were plated in 96-well plates in triplicates, and cell proliferation was measured at 0, 24, 48, 72, and 96 h using the CCK-8 kit following the manufacturer's protocol (CK04-11, Dojindo Laboratories). Average adjusted absorbance from three independent experiments was reported for the analysis.

Animal model

The breast cancer xenograft experimental protocol involving live animals was approved by the Ponce Health

Sciences University Institutional Animal Care and Use Committee (IACUC) protocol number 1908000082. NSG males and females (four weeks old) were obtained from Jackson Laboratories, Inc. (005557). Mice were allowed two weeks of adaptation under a sterile and pathogen-controlled environment with food and distilled water ad libitum before starting breeding. The animals were housed five per cage under constant environmental conditions with 12-h light-dark cycle and unrestricted access to food (standard laboratory mice chow) and water throughout the study. Pain and discomfort were minimized using inhalation anesthesia for surgical procedures. Animals were observed daily by staff, including veterinary supervision. The parameters to determine the study's humane endpoint were determined based on the failure to groom, move or feed, or when tumor volume reached 10% or more of body weight. None of the mice were excluded from the study.

Breast cancer xenograft model

MDA-MB-231 (shRNA Control or shRNA E2F3) cells in their exponential growth phase were washed with $1\times$ PBS and harvested with Trypsin-EDTA 0.25%. A total of 2.5×10^6 viable cells suspended in $50\,\mu L$ of sterile $1\times$ PBS were mixed with $100\,\mu L$ of Matrigel (354234, Corning). Cells were injected into both flanks at the mammary fat pad of 8–10 weeks female NSG mice. The NSG mice harbor two mutations.[26,27] The first renders these mice B and T cell-deficient. The second mutation is a complete null allele of the IL2 receptor common gamma chain (IL2rgnull) that prevents cytokine signaling through multiple receptors, leading to a deficiency in functional NK cells. The lack of immunity allowed us to use the orthotopic method to the effects of E2F3 depletion in metastasis from the mammary glands to distant sites. The control group ($n=10$) received MDA-MB-231 cells previously infected with non-target control transduction particles at a multiplicity of infection (MOI) of 10 (SHC002V, Sigma). The experimental group ($n=10$) received MDA-MB-231 cells previously infected with MISSION shRNA transduction particles that target E2F3 (TRCN0000013807 NM_001949 pLKO.1) (SHCLNV, Sigma). All the animal procedures were carried out under anesthesia using a mix of 2% isoflurane and oxygen delivered by mask. Mice were monitored during recovery and daily after the surgery. Tumors were measured and recorded 20 days post-injection. Both length and width of the tumor were measured two times per week by using a digital caliper. Tumor volume was calculated using the formula: $V=(L \times W^2)/2$, where L represents the larger diameter and W represents the smaller diameter. Eight weeks post-injection, animals were euthanized by inhalation of CO_2. Tumors, spleen, liver, kidneys, lungs, heart, and brain were removed and either frozen in liquid nitrogen or fixed in 10% formalin for further analysis.

India ink

The trachea of the euthanized animal was exposed by removing tissue and muscles. Two threads were placed behind the trachea; the first one was firmly tied as high as possible, while the lower thread was tied without tightening the knot. Using a 1 mL syringe, we performed an intra-tracheal injection of 15% India ink between the two knots until the lungs were completely stained with the solution. After cutting the trachea and removing the lungs from the mouse, the lungs were placed in Fekete's solution (580 mL 100% ethanol, 80 mL formalin, 40 mL glacial acetic acid, and 200 mL dH_2O) overnight at 4°C. White tumor nodules (metastatic foci) were counted visually using a dissection microscope.

Tissue processing and H&E staining

The brain, liver, primary, and secondary tumor samples were all fixed in 10% formalin buffer and embedded in paraffin, as previously described.[28] Paraffin-embedded tissue was sectioned at a thickness of 5 μm. Standard hematoxylin and eosin (H&E, Thermo Fisher, Waltham, MA) staining was performed on formalin-fixed and paraffin-embedded tissue. Images were taken at a magnification of $40\times$, $200\times$, and $400\times$ using the Nikon DS-Ri2 microscope. A certified pathologist at Ponce Health Sciences University (Dr. A. Isidro) examined the stained tissues to assess microscopic and morphologic changes.

Statistical analysis

GraphPad Prism version 8.4.3 (686) was used to analyze the data. Values are represented as mean $\pm$SEM for $n=3$ experiments for all *in vitro* experiments and $n=10$ mice per group for *in vivo* experiments. The data were considered significant if the P-value was <0.05. Student t-test (unpaired, two-tailed) was used to compare differences between groups.

Results

E2F3 and SGO1 are overexpressed in breast cancer and correlate with poor clinical outcomes and EMT gene signatures

To analyze the relationship between E2F3 and SGO1 gene expression and breast cancer patient survival, we used the Kaplan–Meier plotter database.[25] We queried our genes of interest (E2F3 and SGO1) in the mRNA breast cancer database that encompasses data from 4929 patients. This open file database describes the association between E2F3 or SGO1 and the different survival outcomes such as relapse-free survival (RFS), overall survival (OS), distant metastasis-free survival (DFMS), and post-progression survival (PPS). We used the Affymetrix 203693_s_at probe for E2F3 and the Affymetrix 231938_at probe for SGO1. We split the data by median and we did not restrict the analysis by subtypes. We found that high E2F3 mRNA in breast cancer patients correlates significantly with poor RFS, OS, DFMS, and PPS (Supplementary Figure 1(a) to (d)). Meanwhile, elevated SGO1 expression correlates with poor OS, DMFS, and PPS (Supplementary Figure 2(a) to (d)). Further, we compared the mRNA expression of E2F3 and SGO1 in invasive ductal breast cancer versus normal

breast tissue. For this, we used two databases available in Oncomine:[29] Curtis (METABRIC) and TCGA. Using both databases, we found that E2F3 or SGO1 expression was significantly higher on invasive ductal breast cancer than in normal breast (Supplementary Figure 3(a) to (d)).

We then explored if protein–protein interactions have been reported or predicted between E2F3, SGO1, and specific EMT genes. For this, we performed an in silico assay using STRING.[30] We explored correlations between E2F3, SGO1, E2F1, E2F2, Rb, Hec1 (also known as NDC80), Bub1, β-Catenin (CTNNB1), E-Cadherin (CDH1), N-Cadherin (CDH2), Vimentin (VIM), Zeb1, Zeb2, Snail (SNAI1), Slug (SNAI2), Twist1, ZO1 (also known as TJP1), Fibronectin (FN1), Aurora A, Aurora B, and MMPs 2 (MMP2), 3 (MMP3), and 9 (MMP9). We reported evidence, confidence, and molecular action for the queried proteins (Supplementary Figure 4(a) to (c)). We did not find evidence linking directly E2F3 with SGO1 or any of these two with the selected EMT genes. However, there is a link between E2F3 and SGO1 through Bub1 or the Auroras kinases (A or B). Likewise, E2F3 is linked indirectly with EMT genes (specifically β-catenin and E-Cadherin) through other E2Fs or Rb. This information was helpful for target selection for the EMT analysis.

To identify if E2F3 or SGO1 overexpression is correlated with a specific molecular subtype, we performed a bioinformatic analysis using the METABRIC database, which encompasses 2509 patients and the PanCancer TCGA database that encompasses 1084 patients, using the cBioPortal web tool[31] (Tables 1 and 2). We queried the data for E2F1, E2F2, E2F3, and SGO1. We found that E2F3 is the most overexpressed E2F activator in both datasets and is highly overexpressed in TNBC/basal patients (42% in METABRIC and 45% in TCGA). Similarly, SGO1 was highly overexpressed in breast cancer, with a notably high expression in TNBC/basal patients (30% in METABRIC and 20% in TCGA).

To confirm this data, we investigated the expression levels of E2F3 and SGO1 in breast cancer tissue from breast cancer patients with different subtypes (Figure 1(a)

to (c)). Here, we can notice that nuclear SGO1 is significantly overexpressed in breast cancer compared to normal adjacent tissue regardless of hormone receptor status. However, no significant changes were noticed for nuclear E2F3. Taken together, these data suggest that E2F3 and SGO1 could serve as predictors of survival outcomes in breast cancer. Furthermore, E2F3 and SGO1 may serve as predictors of TNBC/basal subtypes and as a clinical target. These data give validity to our premise that E2F3 and SGO1 may be relevant in the progression of TNBC, perhaps by driving early stages of metastasis, and thus, we investigated this relationship experimentally.

E2F3 overexpression leads to SGO1 upregulation, signals EMT, and promotes cell invasion and migration in non-tumorigenic mammary epithelial cells
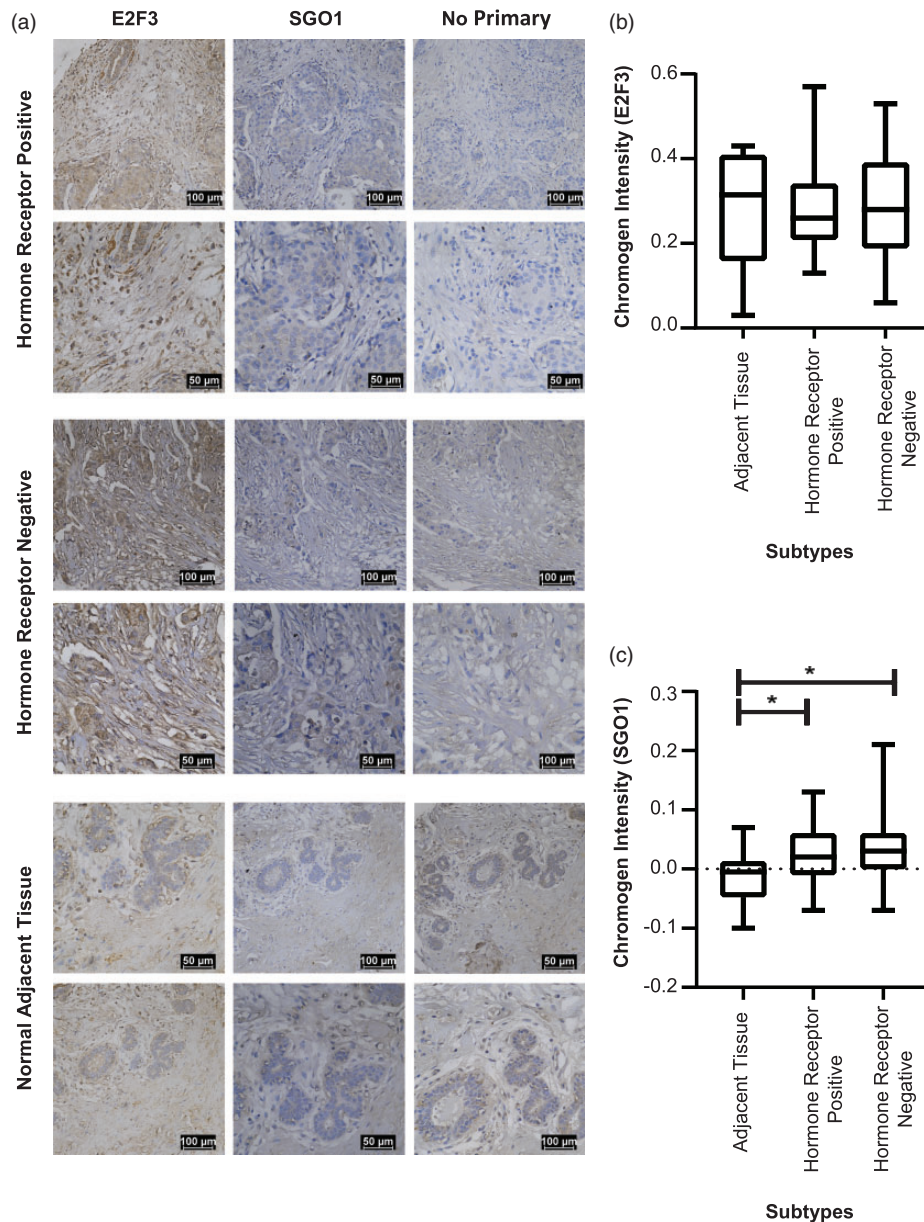
The data presented above show that E2F3 and SGO1 high expression correlates with poor survival outcomes and EMT signatures. Therefore, we investigated the molecular mechanisms by which E2F3 may drive EMT. Previously, we showed that ectopic expression of E2F3 in MCF10A mammary epithelial cells results in the upregulation of SGO1,[19] which was further confirmed in this study (Figure 2(a)). However, the effects of E2F3 overexpression in EMT signaling in breast cancer are unknown. Here we showed that E2F3 overexpression led to changes in EMT protein expression (Figure 2(a)), such as the upregulation of the EMT transcription factors Slug, Snail, and Twist1 as well as an increase in the mesenchymal markers N-Cadherin and Vimentin. Moreover, ectopic expression of E2F3 resulted in decreased levels of the epithelial markers E-Cadherin and ZO-1. Further, E2F3 overexpression in the mammary epithelial cell line MCF10A promotes cell invasion and migration (Figure 2(b) to (d)). Taken together, these data suggest that E2F3 expression is sufficient to induce SGO1 upregulation, EMT signaling, cell invasion, and migration. The data suggest that SGO1 is a critical mediator of these abnormal phenotypes downstream of dysregulated E2F3 expression.

Table 1. Expression of the E2Fs activators and SGO1 in breast cancer (METABRIC).

	Overall (%)	Basals (n = 198) (%)	Her2+ (n = 218) (%)	Luminal A (n = 673) (%)	Luminal B (n = 454) (%)
E2F1	3	5	4.1	0.15	3.96
E2F2	2.8	20	4.6	0	0.66
E2F3	7	42	7.3	0.59	2.42
SGO1	1.5	30	5.96	0.15	6.3

Table 2. Expression of the E2Fs activators and SGO1 in breast cancer (TCGA).

|	Overall (%)	Her2-ER-PR- (n = 55) (%)	Her2+ER-PR- (n = 23) (%)	Her2-ER+PR+ (n = 185) (%)	Her2+ER+PR+ (n = 51) (%)
E2F1	8	29	8.7	4.9	9.8
E2F2	3	1.3	4.3	0	0
E2F3	10	45.5	3.6	1.6	0
SGO1	6	20	5.5	1.1	3.9

Figure 1. SGO1 is significantly overexpressed in breast cancer. E2F3 and SGO1 expression in breast cancer tissue (hormone receptor-positive, $n = 71$ and hormone receptor-negative, $n = 29$) versus normal adjacent tissue ($n = 10$) (a). Images were taken at a 200× (top panels) and 400× (bottom panels) magnification. Scale bars = 100 μm for the 200× and 50 μm for the 400× magnified images. Nuclear E2F3 (b) or SGO1 (c) expression was reported. Error bars represent mean ± SEM. *$P < 0.05$, **$P < 0.01$, and ***$P < 0.001$ were considered statistically significant. Student t-test (unpaired, two-tailed) was used to compare differences between groups. (A color version of this figure is available in the online journal.)

E2F3 and SGO1 silencing modulates EMT in TNBC cells

Knowing that E2F3 overexpression is sufficient to change protein levels of certain EMT targets in mammary epithelial cells, we proceeded to investigate how E2F3 silencing might affect levels of these EMT proteins in TNBC cells. Therefore, we used RNA interference to silence E2F3 or SGO1 using 4-siRNA pools against different regions of their mRNAs in two TNBC cell lines that despite having the same molecular subtypes were isolated from distinct sites. MDA-MB-231 cells were isolated from the ascites fluid of a TNBC patient (a metastatic site), while Hs578t was isolated from the primary tumor of a TNBC patient.[32] After silencing E2F3 or SGO1, we conducted Western blot

analyses. Our data show that E2F3 and SGO1 silencing restores the expression of the epithelial markers E-Cadherin and ZO-1 while decreasing the expression of the EMT transcription factors Snail and Twist1 in MDA-MB-231 cells (Figure 3(a)). Some, but not all, of these findings were corroborated in Hs578t cells (Figure 3(b)). For example, we observed a decrease in Snail expression upon E2F3 or SGO1 silencing, but only SGO1 silencing led to increased levels of E-Cadherin. However, unlike MDA-MB-231 cells, Hs578t cells showed a decrease in Vimentin expression upon silencing of SGO1. On the other hand, immunofluorescence analysis indicates that the silencing of E2F3 in MDA-MB-231 cells increased
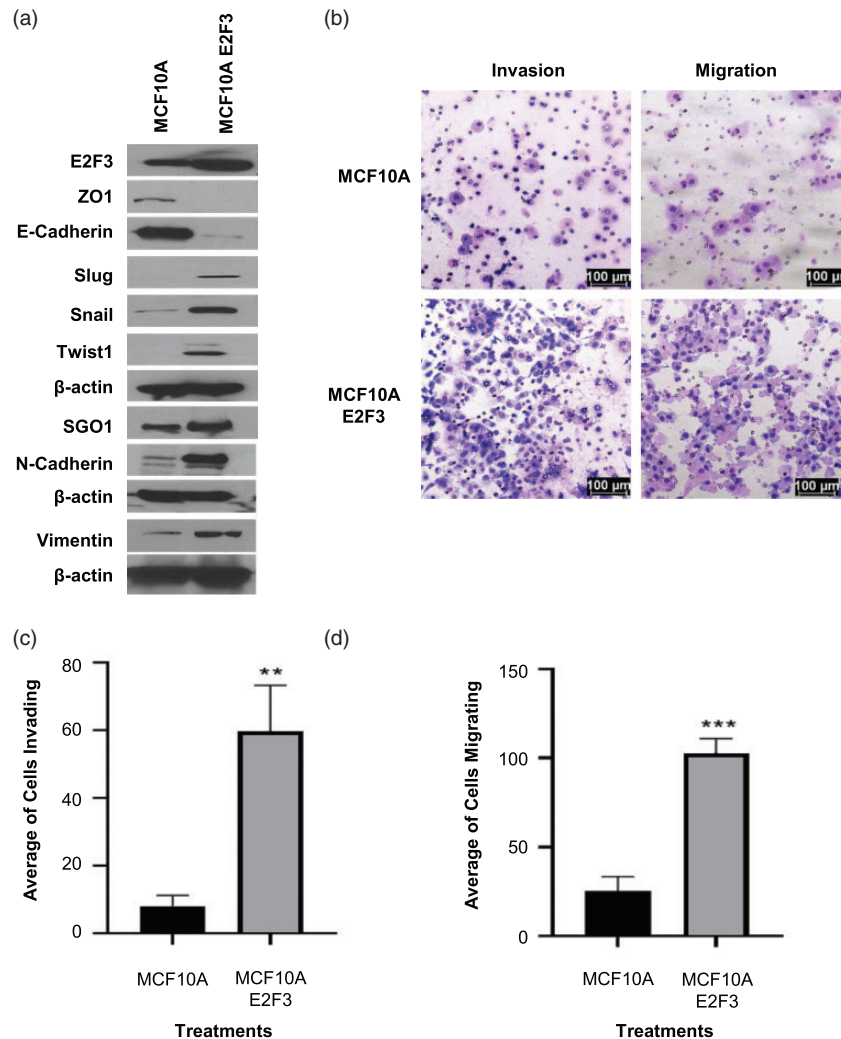
Figure 2. E2F3 overexpression leads to SGO1 overexpression, signals EMT, and promotes cell invasion and migration in non-tumorigenic MCF10A cells. Western blot showing E2F3 characterization and EMT signaling after E2F3 was overexpressed (a). Representative images of MCF10A expressing vector control or MCF10A cells expressing E2F3 that invaded or migrated in the Boyden chamber assay (b). Images were taken at a $200\times$ magnification. Scale bars $= 100\,\mu m$. Three independent experiments were conducted, and the average of the triplicates is shown for cell invasion (c) and migration (d). Error bars represent mean $\pm$ SEM. $*P < 0.05$, $**P < 0.01$, and $***P < 0.001$ were considered statistically significant. Student t-test (unpaired, two-tailed) was used to compare differences between groups. (A color version of this figure is available in the online journal.)

levels of E-cadherin and decreased levels of Vimentin (Figure 3(c)). On the other hand, when SGO1 was silenced, E-cadherin levels were restored, and Vimentin levels were elevated (Figure 3(c)). There were also changes in cellular morphological appearance since MDA-MB-231 cells appear to be more round and epithelial-like after SGO1 silencing. For Hs578t cells, we do not observe changes when E2F3 is downregulated but, consistent with results from the Western blots, we observed a slight increase in E-cadherin expression when SGO1 is downregulated (Figure 3(d)).
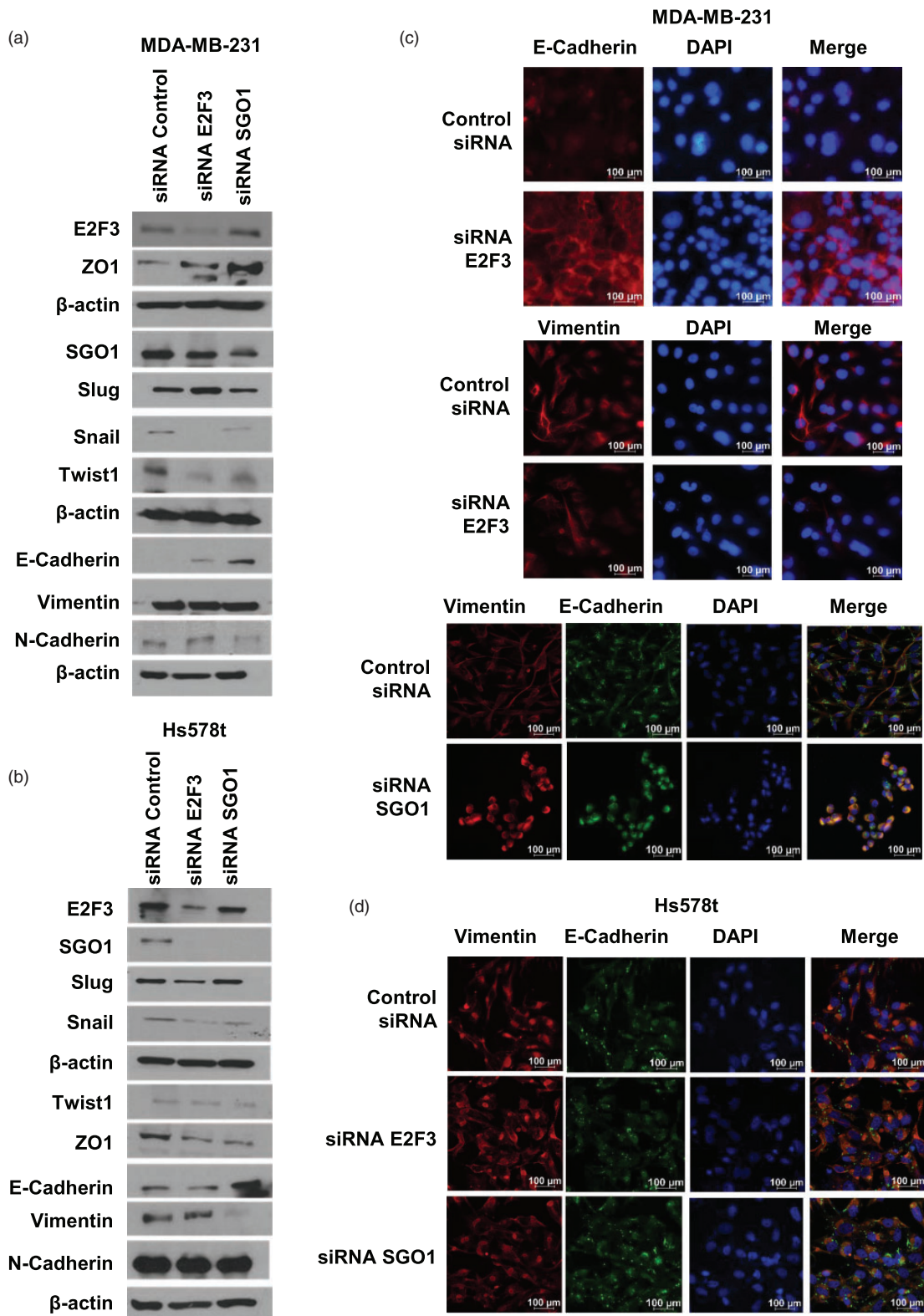
E2F3 and SGO1 silencing reduces cell invasion and migration in TNBC cells

We observed a significant reduction in cell invasion and cell migration after E2F3 or SGO1 silencing in MDA-MB-231 (Figure 4(a) to (c)) and cell invasion and migration after SGO1 silencing, but only a significant reduction in invasion upon E2F3 silencing in Hs578t cells (Figure 4(d) to (f)). Suppression of rates of cell invasion in MDA-MB-231

cells may be explained by the significant reductions in MMP2 and MMP3 expression after silencing E2F3 or SGO1 (Figure 4(g)). Figure 4(h) shows a significant reduction in MMP3 and MMP9 expression only when E2F3 is silenced in Hs578t cells. Taken together with the data presented in Figure 3, these data confirm that E2F3 and SGO1 are important for EMT signaling, cell invasion, and cell migration. Perhaps cell invasion is promoted by MMP upregulation.

MMP3 and Snail silencing reduces cell invasion and migration in TNBC cells

Both MMP3 and Snail have been shown to exert a role in cell invasion and EMT, respectively. We silenced Snail because its levels decreased in MDA-MB-231 and Hs578t cells after E2F3 or SGO1 silencing (Figure 3). We silenced MMP3 since its levels are modulated upon depletion of E2F3 and SGO1 in MDA-MB-231 cells and by E2F3 in Hs578t cells (Figure 4). Snail is a transcription factor that

Figure 3. E2F3 and SGO1 signal EMT in TNBC cells. Western blot showing EMT signaling in MDA-MB-231 (a) and Hs578t (b) cells after E2F3 or SGO1 silencing. Representative immunofluorescence images of E-Cadherin and Vimentin protein expression and localization in MDA-MB-231 (c) and Hs578t (d) cells after E2F3 or SGO1 silencing. Images were taken at a magnification of 600×. Scale bars = 100 μm. (A color version of this figure is available in the online journal.)

negatively regulates cell adhesion molecules such as E-Cadherin, while MMP3 as a metalloproteinase degrades the ECM to promote cell invasion. Therefore, we confirmed that these two EMT genes mediated cell invasion and migration in TNBC cells MDA-MB-231 and Hs578t and that they are important downstream effectors of E2F3 and SGO1 in mediating these abnormal phenotypes (Figure 5(a) to (h)).
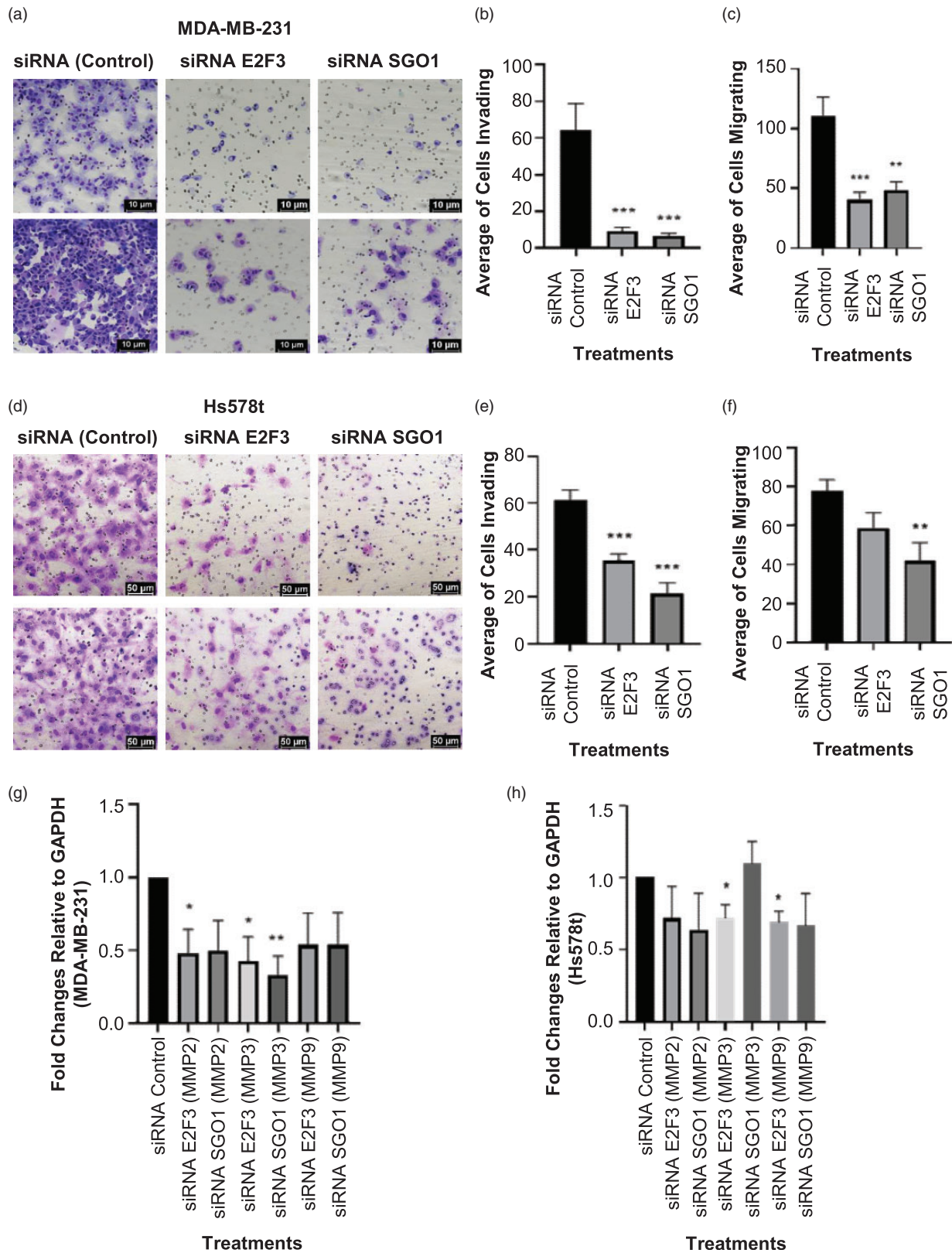
Figure 4. E2F3 and SGO1 promote cell invasion and migration in TNBC cells. Representative images of MDA-MB-231 cells that invaded (top panel) or migrated (bottom panel) in the Boyden chamber assay after being treated with a scrambled siRNA sequence, siRNA E2F3, or SGO1 (a). Images were taken at a 200× magnification. Scale bars = 10 μm. Graphs represent the average of triplicates of cells that invaded (b) and migrated (c). Representative images of Hs578t cells that invaded (top panel) or migrated (bottom panel) in the Boyden chamber assay after being treated with a scrambled siRNA sequence, siRNA E2F3, or SGO1 (d). Images were taken at a 200× magnification. Scale bars = 50 μm. Graphs represent the average of triplicates of cells that invaded (e) and migrated (f). Graphs showing the average of triplicates of MMPs mRNA expression (MMP2, MMP3, and MMP9) in MDA-MB-231 cells (g) and Hs578t (h) cells after E2F3 or SGO1 depletion. Error bars represent mean ± SEM. *$P < 0.05$, **$P < 0.01$, and ***$P < 0.001$ were considered statistically significant. Student *t*-test (unpaired, two-tailed) was used to compare differences between groups. (A color version of this figure is available in the online journal.)
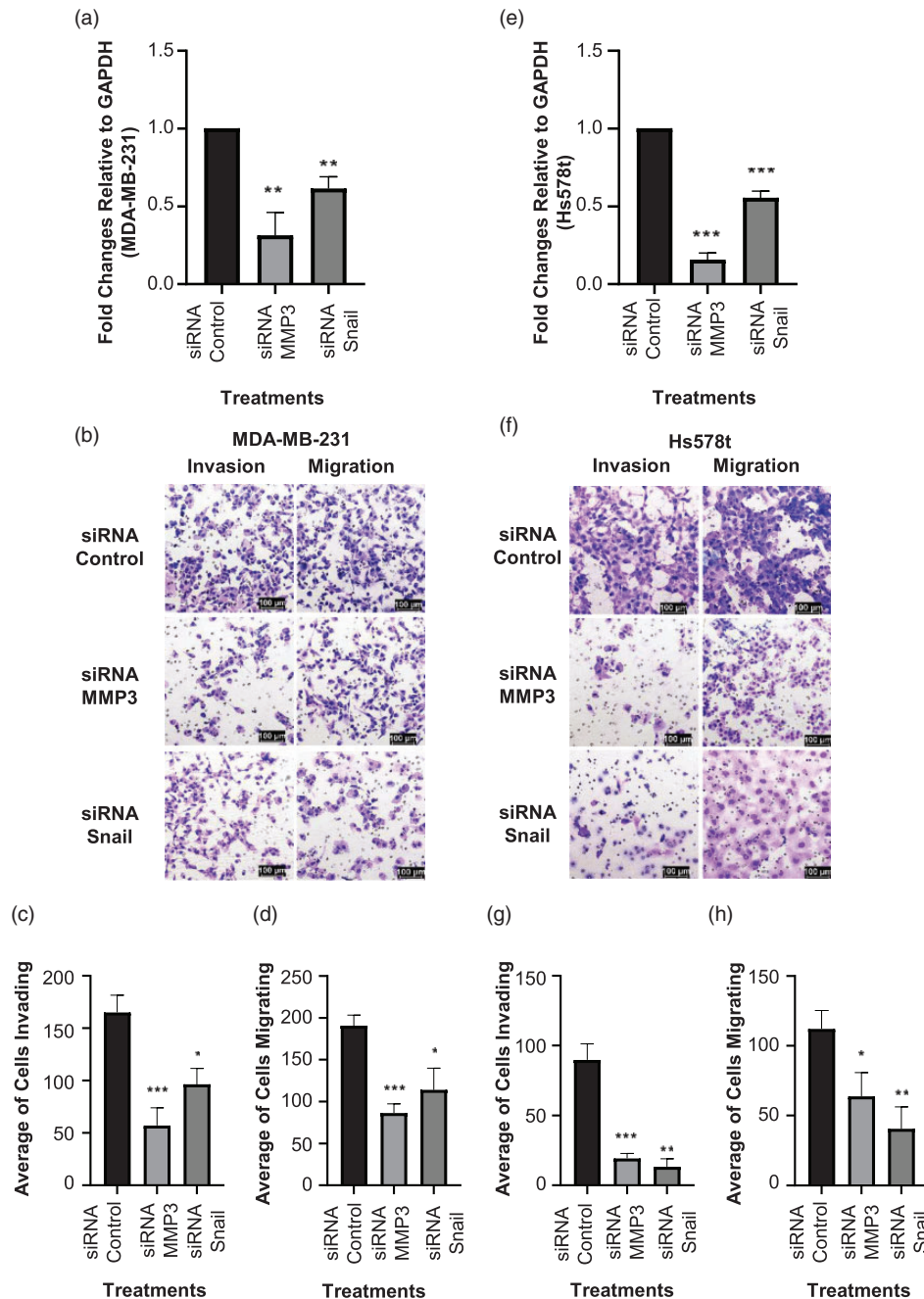
Figure 5. MMP3 and Snail silencing reduce cell invasion and migration in TNBC cells. Characterization of MMP3 and Snail silencing in MDA-MB-231 cells (a). Representative images of MDA-MB-231 cells that invaded or migrated in the Boyden chamber assay after being treated with a scrambled siRNA sequence, siRNA MMP3, or Snail (b). Images were taken at a 200× magnification. Scale bars = 100 µm. Graphs represent the average of triplicates of cells that invaded (c) and migrated (d). Characterization of MMP3 and Snail silencing in Hs578t cells (e). Representative images of Hs578t cells that invaded or migrated in the Boyden chamber assay after being treated with a scrambled siRNA sequence, siRNA MMP3, or Snail (f). Images were taken at a 200× magnification. Scale bars = 100 µm. Graphs represent the average of triplicates of cells that invaded (g) and migrated (h). Error bars represent mean ± SEM. *$P < 0.05$, **$P < 0.01$, and ***$P < 0.001$ were considered statistically significant. Student t-test (unpaired, two-tailed) was used to compare differences between groups. (A color version of this figure is available in the online journal.)

E2F3 depletion reduces cell invasion and migration in MDA-MB-231 cells

Because the siRNA experiments described above transiently suppressed E2F3, we inquired if reduced cell invasion and migration were maintained with long-term inhibition of E2F3. MDA-MB-231 shRNA E2F3 cells were developed and characterized (Figure 6(a)). We confirmed the effects of E2F3 silencing in cell invasion and cell migration and obtained similar results as those with siRNA silencing (Figure 6(b) to (d)). Moreover, stable depletion of E2F3 also resulted in significant reductions in MMP2 and MMP3 mRNAs (Figure 6(e)). Further, we evaluated the
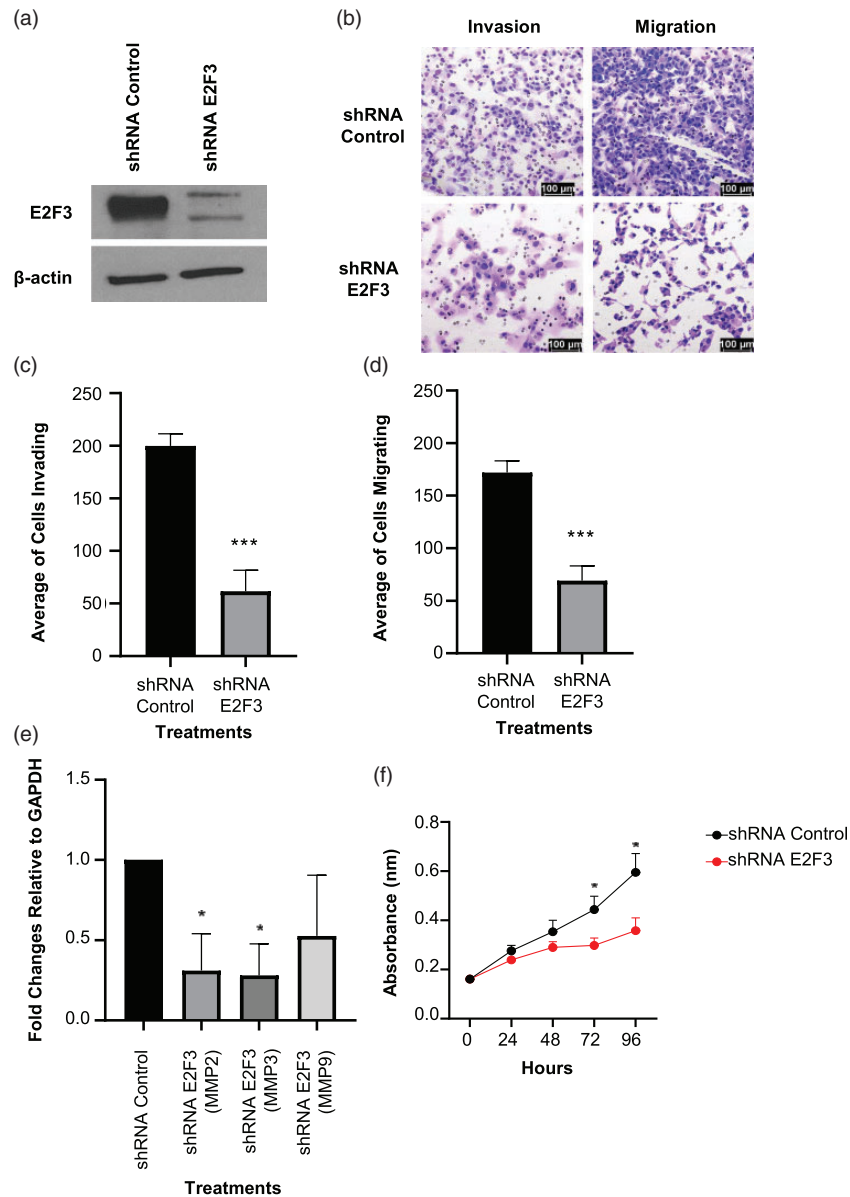
Figure 6. Characterization of shRNA E2F3 and its effects on MMPs, cell invasion, and migration. Western blot characterization of shRNA E2F3-mediated knockdown in MDA-MB-231 cells (a). Representative images of shRNA vector control or shRNA E2F3 MDA-MB-231 cells that invaded or migrated in the Boyden chamber assay (b). Images were taken at a 200× magnification. Scale bars = 100 μm. (c) Graphs represent the average of triplicates of cells that invaded (c) and migrated (d). Graphs represent the average of triplicates of MMP mRNA expression (MMP2, MMP3, and MMP9) in shRNA Control or shE2F3 of MDA-MB-231 cells (e). Graph showing the average cell proliferation and viability for MDA-MB-231 cells treated with shRNA E2F3 compared to shRNA Control (f). Error bars represent mean ± SEM. *$P < 0.05$, **$P < 0.01$, and ***$P < 0.001$ were considered statistically significant. Student *t*-test (unpaired, two-tailed) was used to compare differences between groups. (A color version of this figure is available in the online journal.)

effects of E2F3 depletion in cell proliferation and observed a moderate, but significant decrease in cell proliferation after 72 h (Figure 6(f)).

E2F3 depletion reduces tumor growth and metastasis in NSG mice

MDA-MB-231 cells (either shRNA Control or shRNA E2F3) were injected in NSG mice to observe the effects of E2F3 depletion in TNBC metastasis. Here we showed that E2F3 depletion is retained in the primary tumor (Figure 7(a)). A representative image of primary tumors is shown in Figure 7(b). Images of most of the remaining primary tumors recovered from both groups of mice are shown in

Supplementary Figure 5(a). Interestingly, we showed that E2F3 depletion significantly reduces tumor growth rates (Figure 7(c)), although the changes are moderate. Moreover, secondary tumors were isolated from the axillary lymph nodes. Even though secondary tumors retained the E2F3 depletion (Figure 7(d)), no significant changes were observed in the tumor volume of the metastatic tumors harvested (Figure 7(e)). Interestingly, E2F3 depletion reduced metastasis to the liver (Figure 8(a)). As assessed by the pathologist, 6 out of 10 mice from the control group showed micrometastasis, while none of the mice from the experimental group (shRNA E2F3) exhibited micrometastasis. Moreover, E2F3 depletion reduced lung
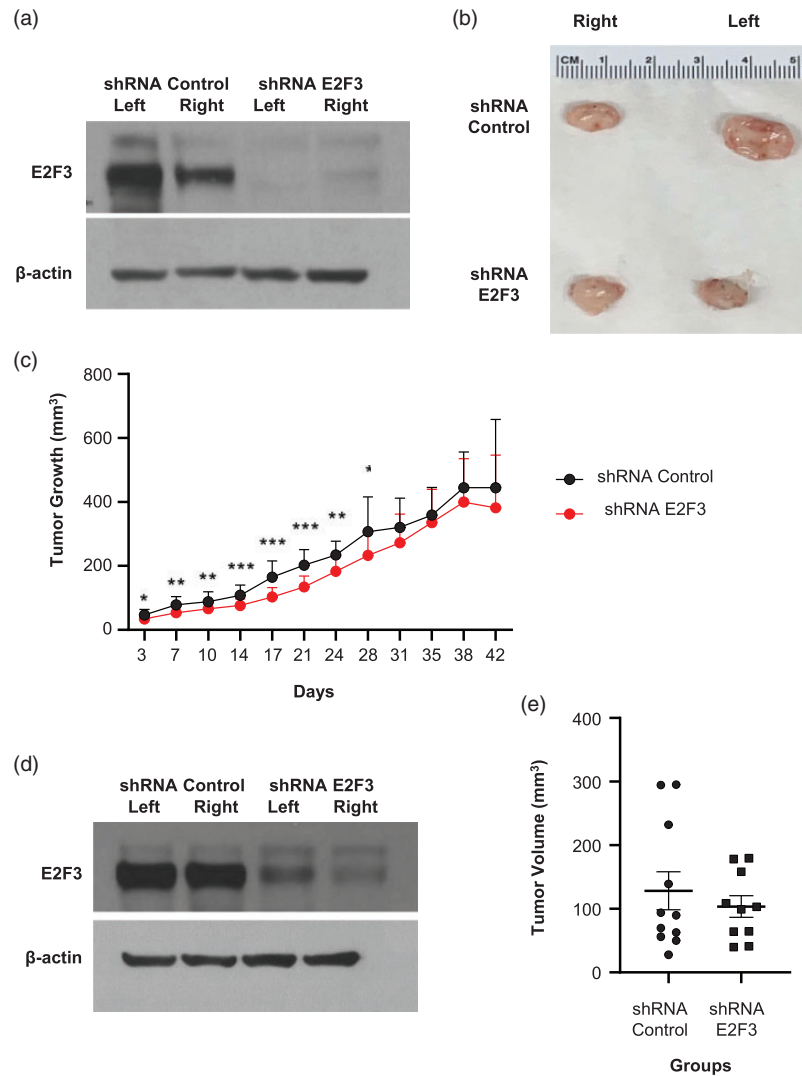
Figure 7. E2F3 depletion reduces tumor growth in NSG mice. Western blot showing E2F3 expression in representative primary tumors (a). Representative images of primary tumors per each group extracted after euthanasia (b). Tumor growth in NSG mice. The graph represents the average of left and right tumors per day for the shRNA Control group ($n = 10$) and the shRNA E2F3 group ($n = 10$) (c). Western blot showing E2F3 expression in representative secondary tumors harvested from axillary lymph nodes (d). Graph showing tumor volume of secondary tumors within lymph nodes (e). Error bars represent mean $\pm$ SEM. *$P < 0.05$, **$P < 0.01$, and ***$P < 0.001$ were considered statistically significant. Student *t*-test (unpaired, two-tailed) was used to compare differences between groups. (A color version of this figure is available in the online journal.)

metastasis significantly (Figure 8(b) and (c)). We also evaluated the effects of E2F3 depletion in breast cancer metastasis to the brain; however, we did not detect brain metastasis in any of the groups (Supplementary Figure 5 (b)). Importantly, loss of E2F3 did not have a general effect on the mice's appearance or their body weight (Supplementary Figure 5(c)). These results suggest an important role for E2F3 in tumor growth as well as lung and liver metastasis of TNBC.

Discussion

TNBC continues to be an especially deadly subtype due to a lack of effective biological therapies. Also, they are prone to become chemoresistant and radioresistant relative to luminal subtypes. Here we evaluated the effects of E2F3 and SGO1 in EMT, cell invasion, cell migration as drivers of metastasis of TNBC cells. Our findings suggest that E2F3

or SGO1 may serve as therapeutic targets in efforts to develop novel therapies in TNBC. Alternatively, kinases that regulate SGO1 expression (like Aurora B, Bub1, Nek2, or TTK)[33] can be targeted with small molecule inhibitors, and some of them are currently in clinical trials. This is the first study that shows a role for SGO1 and E2F3 in EMT and cell invasion in TNBC.

We found that high E2F3 or SGO1 expression correlates significantly with poor survival outcomes, including RFS, OS, DMFS, and PPS. We also showed that E2F3 and SGO1 expression is higher in invasive ductal breast cancer than normal breast tissue. We further showed that SGO1 but not E2F3 expression is higher in breast cancer relative to patient tissue. This highlights an important distinction between E2F3 and SGO1, since SGO1 may be an important predictor for advanced breast tumors, including TNBC. The presence of E2F3 in both tumors and adjacent tissue may be reflective of E2F3b's essential nature as a transcriptional repressor.
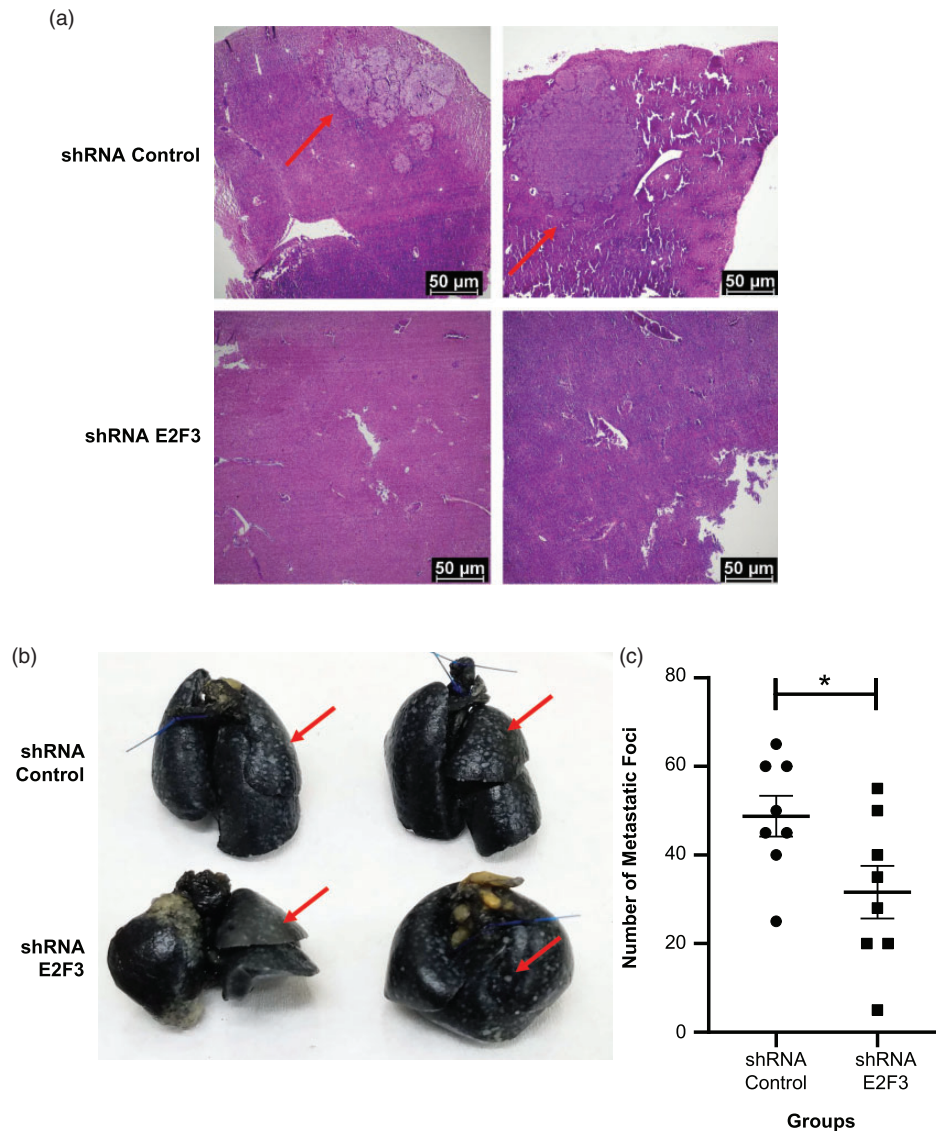
Figure 8. E2F3 depletion reduces metastasis to the liver and lungs mic. Representative images for H&E staining of liver from two independent mice per group (a). The red arrows point to micrometastasis. Images were taken at a 40× magnification. Scale bars = 50 μm. Representative images of mice lungs (posterior view) stained with India Ink from two independent mice per group (b). Red arrows point to white nodules (metastatic foci) that were counted. The graph represents the average for each group (c). Error bars represent mean ± SEM. *P < 0.05, **P < 0.01, and ***P < 0.001 were considered statistically significant. Student *t*-test (unpaired, two-tailed) was used to compare differences between groups. (A color version of this figure is available in the online journal.)

No one so far has been able to design antibodies that distinguish the activator (E2F3a) from the repressor (E2F3b), since they only differ in six amino acids.[32] Also, E2F3 is important to the microenvironment since its deletion in macrophages suppresses metastasis to the lungs.[34] Despite this important distinction, we found that both E2F3 and SGO1 signal some EMT genes and have an important role in cell invasion and cell migration. Two genes that were consistently affected by the E2F3 and SGO1 silencing were Snail and MMP3. Snail is a transcription factor that represses E-Cadherin.[10] The loss of E-Cadherin is an important hallmark of EMT that leads to loss of cellular adhesions, cell polarity, and promotes invasion. EMT is a precursor of metastasis, which ultimately is what affects patient survival. MMP3 is another important protein involved in cell invasion since it can degrade ECM components such as fibronectin, laminin, gelatins of type I, III, IV,

and V; collagens III, IV, X, and IX, and cartilage proteoglycans, thus facilitating invasion.[35] Furthermore, high expression of MMP3 in breast cancer brain metastasis has been reported (along with MMP2 and MMP9).[36] Similarly, MMPs have been shown to regulate the tumor microenvironment to facilitate cell invasion, intravasation, and metastatic niche formation. MMPs have been shown to aid in cell growth, cell survival, angiogenesis, and inflammation. This along with other effects on the tumor microenvironment can be reviewed in Kessenbrock *et al.*[37] Furthermore, we found that E2F3 depletion reduces tumor growth and metastasis (in lungs and liver) in NSG mice, highlighting the importance of E2F3 and its downstream targets in TNBC.

Our study shows a promising link between E2F3, SGO1, EMT, and metastasis in TNBC. One limitation that our study had is that we did not evaluate the consequences of

SGO1 depletion in metastasis in TNBC. SGO1 depletion may reduce metastasis given the fact that SGO1 does regulate cell invasion and migration *in vitro.* Also, SGO1 may reduce tumor growth (and thus metastasis) due to its role in chromosome cohesion during mitosis by preventing premature dissociation of cohesin complex from centromeres after prophase.[38] However, the effects of SGO1 in metastasis need to be validated *in vivo.* Potential avenues for future studies may include showing if E2F3 regulates other kinases that have been shown to regulate SGO1 (i.e., TTK, Aurora B, or BUB1) and target these kinases in metastasis in TNBC. Our group showed that two kinases that phosphorylate SGO1 (Nek2 and TTK) are under the direct control of E2F1, E2F2, and E2F3, and mediate EMT, cell invasion, and migration so perhaps they can be targeted to modulate E2F3 activity in TNBC breast cancer. Targeting any of these kinases may be more feasible than targeting E2F3 or SGO1. Already some inhibitors for Aurora B are in clinical trial phases (this can be further reviewed in Colón-Marrero *et al.*[24]) Also, some studies have shown a role for some of these kinases in EMT and metastasis in breast cancer. For example, Aurora B has been shown to induce EMT via OCT4/AKT/GSK3β/Snail1 signaling.[39] Moreover, Aurora B depletion has been shown to reduce tumor growth and metastasis to the lung.[39]

In conclusion, our findings suggest that E2F3 and SGO1 play a novel role in TNBC by regulating EMT, cell invasion, and cell migration, through Snail and MMP3. Further, our findings suggest a key role for E2F3 in metastasis in TNBC.

AUTHORS' CONTRIBUTIONS

SJ, YRR, CCC, AJRJ, JVV, AI, MECR, and HIS conducted experiments and/or performed data analysis. AI is a board-certified pathologist who conducted the pathological analysis. MBC and GNAP conducted the breeding and provided the animals. SJ wrote the manuscript. YRR, CCC, MBC, GNAP, and HIS edited the manuscript. SJ and HIS conceived the idea and provided an overall experimental design. All authors read and approved the final manuscript.

ACKNOWLEDGMENTS

DECLARATION OF CONFLICTING INTERESTS

FUNDING

ORCID iDs

Armando J Ruiz-Justiz (iD) https://orcid.org/0000-0003-0745-2061
Harold I Saavedra (iD) https://orcid.org/0000-0001-6171-9949

REFERENCES

1. Sung H, Ferlay J, Siegel RL, Laversanne M, Soerjomataram I, Jemal A, Bray F. Global cancer statistics 2020: GLOBOCAN estimates of incidence and mortality worldwide for 36 cancers in 185 countries. *CA Cancer J Clin* 2021;**71**:209–49

2. Kent LN, Leone G. The broken cycle: E2F dysfunction in cancer. *Nat Rev Cancer* 2019;**19**:326–38

3. Andrechek ER. HER2/neu tumorigenesis and metastasis is regulated by E2F activator transcription factors. *Oncogene* 2015;**34**:217–25

4. Godinho SA, Picone R, Burute M, Dagher R, Su Y, Leung CT, Polyak K, Brugge JS, Thery M, Pellman D. Oncogene-like induction of cellular invasion from centrosome amplification. *Nature* 2014;**510**:167–71

5. Lee M, Oprea-Ilies G, Saavedra HI. Silencing of E2F3 suppresses tumor growth of Her2+ breast cancer cells by restricting mitosis. *Oncotarget* 2015;**6**:37316–34

6. Lee MY, Moreno CS, Saavedra HI. E2F activators signal and maintain centrosome amplification in breast cancer cells. *Mol Cell Biol* 2014;**34**:2581–99

7. Saavedra HI, Maiti B, Timmers C, Altura R, Tokuyama Y, Fukasawa K, Leone G. Inactivation of E2F3 results in centrosome amplification. *Cancer Cell* 2003;**3**:333–46

8. Chen HZ, Tsai SY, Leone G. Emerging roles of E2Fs in cancer: an exit from cell cycle control. *Nat Rev Cancer* 2009;**9**:785–97

9. Schaal C, Pillai S, Chellappan SP. The Rb-E2F transcriptional regulatory pathway in tumor angiogenesis and metastasis. *Adv Cancer Res* 2014;**121**:147–82

10. Lamouille S, Xu J, Derynck R. Molecular mechanisms of epithelial-mesenchymal transition. *Nat Rev Mol Cell Biol* 2014;**15**:178–96

11. Thiery JP, Acloque H, Huang RY, Nieto MA. Epithelial-mesenchymal transitions in development and disease. *Cell* 2009;**139**:871–90

12. Thiery JP, Sleeman JP. Complex networks orchestrate epithelial-mesenchymal transitions. *Nat Rev Mol Cell Biol* 2006;**7**:131–42

13. Huang RY, Guilford P, Thiery JP. Early events in cell adhesion and polarity during epithelial-mesenchymal transition. *J Cell Sci* 2012;**125**:4417–22

14. Nistico P, Bissell MJ, Radisky DC. Epithelial-mesenchymal transition: general principles and pathological relevance with special emphasis on the role of matrix metalloproteinases. *Cold Spring Harb Perspect Biol* 2012;**4**:a011908

15. Peinado H, Olmeda D, Cano A. Snail, zeb and bHLH factors in tumour progression: an alliance against the epithelial phenotype? *Nat Rev Cancer* 2007;**7**:415–28

16. Yilmaz M, Christofori G. EMT, the cytoskeleton, and cancer cell invasion. *Cancer Metastasis Rev* 2009;**28**:15–33

17. Barrallo-Gimeno A, Nieto MA. The snail genes as inducers of cell movement and survival: implications in development and cancer. *Development* 2005;**132**:3151–61

18. Zhu QQ, Ma C, Wang Q, Song Y, Lv T. The role of TWIST1 in epithelial-mesenchymal transition and cancers. *Tumour Biol* 2016;**37**:185–97

19. Lee M, Rivera-Rivera Y, Moreno CS, Saavedra HI. The E2F activators control multiple mitotic regulators and maintain genomic integrity through Sgo1 and BubR1. *Oncotarget* 2017;**8**:77649–72

20. King JL, Zhang B, Li Y, Li KP, Ni JJ, Saavedra HI, Dong JT. TTK promotes mesenchymal signaling via multiple mechanisms in triple negative breast cancer. *Oncogenesis* 2018;**7**:69

21. Zhang Y, Wang W, Wang Y, Huang X, Zhang Z, Chen B, Xie W, Li S, Shen S, Peng B. NEK2 promotes hepatocellular carcinoma migration and invasion through modulation of the epithelial-mesenchymal transition. *Oncol Rep* 2018;**39**:1023–33

22. Mu J, Fan L, Liu D, Zhu D. Overexpression of shugoshin1 predicts a poor prognosis for prostate cancer and promotes metastasis by affecting epithelial-mesenchymal transition. *Onco Targets Ther* 2019;**12**:1111–8

23. Rivera-Rivera Y, Marina M, Jusino S, Lee M, Velazquez JV, Chardon-Colon C, Vargas G, Padmanabhan J, Chellappan SP, Saavedra HI. The Nek2 centrosome-mitotic kinase contributes to the mesenchymal state, cell invasion, and migration of triple-negative breast cancer cells. *Sci Rep* 2021;**11**:9016

24. Colon-Marrero S, Jusino S, Rivera-Rivera Y, Saavedra HI. Mitotic kinases as drivers of the epithelial-to-mesenchymal transition and as therapeutic targets against breast cancers. *Exp Biol Med* 2021;**246**:1036–44

25. Nagy A, Munkacsy G, Gyorffy B. Pancancer survival analysis of cancer hallmark genes. *Sci Rep* 2021;**11**:6047

26. Coughlan AM, Harmon C, Whelan S, O'Brien EC, O'Reilly VP, Crotty P, Kelly P, Ryan M, Hickey FB, O'Farrelly C, Little MA. Myeloid engraftment in humanized mice: impact of granulocyte-colony stimulating factor treatment and transgenic mouse strain. *Stem Cells Dev* 2016;**25**:530–41

27. Shultz LD, Lyons BL, Burzenski LM, Gott B, Chen X, Chaleff S, Kotb M, Gillies SD, King M, Mangada J, Greiner DL, Handgretinger R. Human lymphoid and myeloid cell development in NOD/LtSz-scid IL2R gamma null mice engrafted with mobilized human hemopoietic stem cells. *J Immunol* 2005;**174**:6477–89

28. Isidro RA, Isidro AA, Cruz ML, Hernandez S, Appleyard CB. Double immunofluorescent staining of rat macrophages in formalin-fixed paraffin-embedded tissue using two monoclonal mouse antibodies. *Histochem Cell Biol* 2015;**144**:613–21

29. Rhodes DR, Yu J, Shanker K, Deshpande N, Varambally R, Ghosh D, Barrette T, Pandey A, Chinnaiyan AM. ONCOMINE: a cancer microarray database and integrated data-mining platform. *Neoplasia* 2004;**6**:1–6

30. Szklarczyk D, Gable AL, Lyon D, Junge A, Wyder S, Huerta-Cepas J, Simonovic M, Doncheva NT, Morris JH, Bork P, Jensen LJ, Mering CV. STRING v11: protein-protein association networks with increased coverage, supporting functional discovery in genome-wide experimental datasets. *Nucleic Acids Res* 2019;**47**:D607–D13

31. Cerami E, Gao J, Dogrusoz U, Gross BE, Sumer SO, Aksoy BA, Jacobsen A, Byrne CJ, Heuer ML, Larsson E, Antipin Y, Reva B, Goldberg AP, Sander C, Schultz N. The cBio cancer genomics portal: an open platform for exploring multidimensional cancer genomics data. *Cancer Discov* 2012;**2**:401–4

32. Neve RM, Chin K, Fridlyand J, Yeh J, Baehner FL, Fevr T, Clark L, Bayani N, Coppe JP, Tong F, Speed T, Spellman PT, DeVries S, Lapuk A, Wang NJ, Kuo WL, Stilwell JL, Pinkel D, Albertson DG, Waldman FM, McCormick F, Dickson RB, Johnson MD, Lippman M, Ethier S, Gazdar A, Gray JW. A collection of breast cancer cell lines for the study of functionally distinct cancer subtypes. *Cancer Cell* 2006;**10**:515–27

33. Jusino S, Saavedra HI. Role of E2Fs and mitotic regulators controlled by E2Fs in the epithelial to mesenchymal transition. *Exp Biol Med* 2019;**244**:1419–29

34. Trikha P, Sharma N, Pena C, Reyes A, Pecot T, Khurshid S, Rawahneh M, Moffitt J, Stephens JA, Fernandez SA, Ostrowski MC, Leone G. E2f3 in tumor macrophages promotes lung metastasis. *Oncogene* 2016;**35**:3636–46

35. Cui N, Hu M, Khalil RA. Biochemical and biological attributes of matrix metalloproteinases. *Prog Mol Biol Transl Sci* 2017;**147**:1–73

36. Mendes O, Kim HT, Stoica G. Expression of MMP2, MMP9 and MMP3 in breast cancer brain metastasis in a rat model. *Clin Exp Metastasis* 2005;**22**:237–46

37. Kessenbrock K, Plaks V, Werb Z. Matrix metalloproteinases: regulators of the tumor microenvironment. *Cell* 2010;**141**:52–67

38. McGuinness BE, Hirota T, Kudo NR, Peters JM, Nasmyth K. Shugoshin prevents dissociation of cohesin from centromeres during mitosis in vertebrate cells. *PLoS Biol* 2005;**3**:e86

39. Zhang J, Lin X, Wu L, Huang JJ, Jiang WQ, Kipps TJ, Zhang S. Aurora B induces epithelial-mesenchymal transition by stabilizing Snail1 to promote basal-like breast cancer metastasis. *Oncogene* 2020;**39**:2550–67